Evaluating Yangtze River Delta Urban Agglomeration flood risk using hybrid method of AutoML and AHP

Yu Gao [1,2], Haipeng Lu [1,2], Yaru Zhang[1,2], Hengxu Jin[1,2], Shuai Wu[3], Yixuan Gao[1,2], Shuliang Zhang[1,2*]

1 Key Laboratory of VGE of Ministry of Education, Nanjing Normal University, Nanjing 210023, China

2 Jiangsu Center for Collaborative Innovation in Geographical Information Resource Development and Application, Nanjing 210023, China

3 Lianyungang Real Estate Registry, Lianyungang 222006, China

Correspondence to: Shuliang Zhang (zhangshuliang@njnu.edu.cn)

Abstract. With rapid urbanization, the scientific assessment of disaster risk caused by flooding events has become an essential task for disaster prevention and mitigation. However, adaptively selecting optimal machine learning (ML) models for flood risk assessment and further conducting spatial and temporal analyses of flood risk characteristics in urban agglomerations remain challenging. This study, establishes a "H–E–V–R" risk assessment index system that integrates hazard, exposure, vulnerability, and resilience based on the factors influencing flood risk in the Yangtze River Delta Urban Agglomeration (YRDUA). Utilizing Automated Machine Learning (AutoML) and the Analytic Hierarchy Process (AHP), a comprehensive flood risk assessment model is constructed. Results indicate that, among those of different assessment models, the accuracy, precision, F1-score, and kappa coefficient of the Categorical Boosting (CatBoost) model for flooded point identification are the highest. Among the flood hazard factors, elevation ranks highest in importance, with a contribution rate of up to 68.55%. The spatial distribution of flood risk in the study area from 1990 to 2020 is heterogeneous, with an overall increasing risk trend. This study is of great significance for advancing disaster prevention, mitigation, and sustainable development in the YRDUA.

1 Introduction

Under global climate change and accelerated urbanization, China has been experiencing pervasive flooding ever more frequently (Tang et al., 2024). Floods threaten people's lives, hinder social development and cause huge economic losses in China (Anon, 2021; Echendu, 2020; Milanesi et al., 2015). Flood formation has been exacerbated by climate change and urbanization, leading to increased frequency, extent, and intensity of urban flooding, and impacting urban flood risk (Mahmoud and Gan, 2018; Khadka et al., 2023; Scott et al., 2023; Seemuangngam and Lin, 2024). Modern human society is faced with the possibility of serious flood hazards and associated challenges, and in addition to post-disaster emergency management, the scientific assessment of disaster risks arising from flood events has gradually become a crucial aspect in preventing and mitigating disasters.

Currently, most research in the field of flooding focuses on the flood risks of individual cities (Wang et al., 2021, 2023b; Guan et al., 2024). However, in recent years, the frequency and intensity of urban flooding in China have increased dramatically, and individual cities are no longer able to independently mitigate the risks arising from floods. Studies indicate that China's flood risk management needs to be transformed from the scale of isolated individual cities to the scale of urban agglomerations, conducted in a regionally coordinated manner (Morales-Torres et al., 2016; Wang et al., 2023a). City clusters, constituting the spatial organizational structure of cities that have reached an advanced stage of development, have become key areas for regional disaster management and sustainable development. Due to the unique geographical location and climate conditions of the YRDUA, as well as the impact of urbanization over the past 30 years, the frequency and intensity of flood disasters have been increasing, posing a serious threat to the sustainable development of cities. Therefore, implementing relevant emergency management strategies for flood risks is urgently needed. Furthermore, the region comprises multiple cities, among which distinct resource interactions, such as population mobility and risk transfer, exist (Lu et al., 2022). Thus, it is essential to assess both the overall flood risk characteristics and changes in the urban agglomeration, as well as the spatial correlations of flood risks between cities, explore the mutual influences and interaction mechanisms among regional disaster risks, and provide a scientific basis for sustainable development within the urban agglomeration (Xu et al., 2024).

Statistical analyses of historical disaster statistics (Lang et al., 2004), indicator systems methods (Wang et al., 2018b), scenario simulations methods (Yang et al., 2018), and data-driven methods (Abu-Salih et al., 2023), are the primary flood risk assessment method currently. With the development of artificial intelligence technology, data-driven methods, such as machine learning, deep learning, and artificial neural networks, have emerged, providing new opportunities for improving traditional flood risk assessment methods (Liu Jiafu and Zhang Bai, 2015). Ensemble methods are a class of machine learning (ML) techniques that combine multiple base learners to form a stronger predictive model (Webb and Zheng, 2004). They are designed to overcome several limitations of individual models, such as high variance, overfitting, sensitivity to noise, and poor generalization (Yang et al., 2013)Through continuous improvement and development of machine learning algorithms, ensemble methods have effectively addressed the limitations of traditional machine learning models. By aggregating the outputs of weak learners, ensemble methods significantly enhance model stability, accuracy, and robustness—especially

63 in high-dimensional and complex classification or regression tasks (Kazienko et al., 2015). Various

64 ~~integrated~~ensemble ML ~~methods~~techniques, including bagging (e.g., Random Forest), boosting (e.g.,

65 XGBoost, CatBoost), and stacking, have been ~~utilized~~widely used in hydrology, with ~~the Boost algorithm~~

66 ~~being extensively applied for~~boosting algorithms in particular showing strong performance in flood

67 prediction and risk assessment (Shafizadeh-Moghadam et al., 2018; Mirzaei et al., 2021; Yan et al.,

68 2024). However, ~~these integrated models~~ensemble ML techniques often lack preprocessing and feature

69 selection capabilities, and their application effects vary considerably across different regions. To fully

70 mine data and discover more effective features, experts have proposed other solutions, namely hybrid

71 models such as ANFIS, LSTM-ALO, and LSSVM-GSA (Nayak et al., 2004; Yuan et al., 2018; Adnan et

72 al., 2017). These methods have achieved good performances for given hydrological time series, focusing

73 more on data preprocessing and feature selection. Although research on data-driven urban flood risk

74 assessment methods has increased, certain limitations remain. For example, the physical importance of

75 urban hydrological processes is often ignored in the model assessment process, interpretation of the

76 assessment results is weak, and quantifying the boundaries and scales is challenging (Abu-Salih et al.,

77 2023; Guo et al., 2022).

78 Furthermore, attempting to combine the data processing and feature selection capabilities of hybrid

79 models with those of integrated models remains challenging (Li et al., 2017). ~~Existing~~While ML

80 algorithms ~~cannot perform well for~~have demonstrated strong performance in many domains, no single

81 algorithm consistently performs best across all ~~learning~~types of problems (Wolpert and Macready, 1997)~~;~~

82 ~~thus, each ML component, such as~~. Therefore, to achieve optimal performance, it is essential to carefully

83 configure key components of the ML pipeline, including feature engineering, model selection, and

84 ~~algorithm selection, must be carefully configured~~hyperparameter tuning (Li et al., 2017; Raschka, 2020).

85 Hence, ML applications require the participation of many experts, leading to disproportionate costs for

86 ML development and improvement (Wagenaar et al., 2020; Sarro et al., 2022; Rashidi Shikhteymour et

87 al., 2023). The effectiveness of ~~machine learning "automatically~~ML improves with experience~~," and a~~

88 ~~key challenge in~~, where "experience" refers to the ~~research is how to integrate the~~model's iterative

89 exposure to training data ~~processing capabilities and feature selection strengths of hybrid models with~~

90 ~~ensemble models~~and its ability to learn patterns from labeled examples (Jordan and Mitchell, 2015;

91 Nagarajah and Poravi, 2019). One key challenge addressed in this study is how to automatically optimize

92 model components such as feature selection and algorithm configuration in flood risk prediction, while

93 maintaining high accuracy and adaptability across complex hydrological conditions. AutoML is an

94 innovative ML framework that automates key stages of the model development pipeline, including

95 feature selection, model selection, hyperparameter tuning, and ensemble learning (He et al.,

96 2021a)~~AutoML is an innovative ML framework designed for training ML models and addressing various~~

97 ~~problems~~. By addressing these challenges, AutoML reduces reliance on expert knowledge and minimizes

98 subjectivity in model building (He et al., 2021b; Consuegra-Ayala et al., 2022)~~.~~. In the context of this

99 study, AutoML enables the automatic optimization of hazard factor selection, model construction, and

100 parameter adjustment for flood risk assessment tasks, thereby improving efficiency, objectivity, and

101 reproducibility in model development. However, AutoML has not been widely applied in the fields of

102 hydrology and disaster risk management, and research has mainly focused on optimizing the integrated

103 model to achieve better performance (Özdemir et al., 2023). Continuous research has highlighted the

104 potential role of AutoML in flood risk detection and assessment (Guo et al., 2022; Vincent et al., 2023;

105 Munim et al., 2024). Guo et al. (2022) compared AutoML with three single ML algorithms (CatBoost,

106 XGBoost, and BPDNN) and concluded that AutoML performed better in building rapid warning and

107 comprehensive analysis models for urban waterlogging. The model based on AutoML can be applied to

108 areas without water level monitoring and achieve accurate predictions and rapid warnings of

109 waterlogging depth (Guo et al., 2022; Yan et al., 2024). Abu-Salih et al. (2023) proposed a data-driven

110 flood risk area detection model that combined the integrated model with the AutoML tool and

111 successfully solved the problems of data balance and strategy modeling, while reducing the complexity

112 of flood risk area prediction. Previous studies have provided a theoretical basis and scientific reference

113 for the application of AutoML methods to flood risk assessment. However, the use of AutoML for

114 research purposes is a complex issue, and many new opportunities and challenges remain regarding its

115 specific applications.

116 In the field of flood risk assessment, AutoML has been preliminarily demonstrated to perform well in

117 flood hazard prediction (Guo et al., 2022c). As an efficient "black-box" modeling approach, AutoML

118 provides strong support for flood risk modeling through automated feature selection, model training, and

119 parameter optimization (Hutter et al., 2019; He et al., 2021a). In urban agglomerations, flood risk

120 assessment is a highly complex task involving diverse natural and socioeconomic factors derived from

121 heterogeneous and often multi-source datasets (Wang et al., 2023c). These factors—such as rainfall,

topography, land use, drainage, and population density—differ in type and often interact in non-linear and uncertain ways (Shuster et al., 2005; Zhang et al., 2017; Wang et al., 2018a). Under such complex circumstances, AutoML struggles to systematically evaluate the multi-dimensional indicators of flood risk. To address this limitation, this study introduces a multicriteria decision analysis (MCDA) approach to quantify the importance of various indicators within the evaluation framework (Pham et al., 2021). MCDA facilitates the integration of such heterogeneous indicators into a unified evaluation framework by constructing structured weighting schemes, thereby aligning the assessment results more closely with real-world conditions and expert knowledge (Fernández and Lutz, 2010). In cases where data are limited or certain indicators are difficult to quantify, MCDA methods allow for the incorporation of expert judgment through scoring systems and pairwise comparison matrices, enhancing the practical applicability and robustness of the model (Hites et al., 2006)Although AutoML can objectively and efficiently calculate flood risk, it lacks comprehensiveness and judgment. Therefore, when evaluating the indicators of various dimensions of flood risk, quantifying the impacts of different levels of each indicator on flood risk is impossible, and determining the indicator weight is challenging. Therefore, to determine the indicator weight, using relevant statistical methods is necessary. Multicriteria decision analysis (MCDA) is a useful tool for considering complex decision-making problems in flood risk management . The analytic hierarchy process (AHP) is one of the most popular MCDA techniques (Donegan et al., 1992). This technique emphasizes the importance of the subjective judgment of decision makers and the consistency of pairwise comparisons of standards in the decision-making process (Saaty, 1980). Recent studies have focused on integrated frameworks of ML models and MCDA technology for flood hazard assessment (Kanani-Sadat et al., 2019; Khosravi et al., 2019; Gudiyangada Nachappa et al., 2020; Mia et al., 2023). However, research focusing on using an integrated framework of AutoML and AHP techniques is still limited.

This study constructsdevelops a flood risk assessment model based on AutoML and AHP for the YRDUA by examininganalyzing the factors influencing flood risk in the YRDUA. Based onand integrating AutoML and AHP methods. In this model, AutoML is employed to construct the proposedflood hazard sub-model, using indicators that represent natural environmental drivers as input features. The hazard is modeled as a binary classification problem (i.e., whether flooding occurs), and the resulting feature importance rankings provide an objective basis for subsequent indicator weighting. Nevertheless, as a data-driven approach, AutoML alone cannot structurally interpret the relative influence of social and

systemic factors within a multi-dimensional flood risk assessment ~~model, the risk,~~framework. Therefore, this study incorporates the AHP to calculate the weights of flood exposure, vulnerability, and resilience ~~as well as their corresponding weights of flooding~~ in the YRDUA ~~are calculated,~~ based on expert knowledge and ~~the~~existing literature. A regional flood risk ~~level~~zoning map is ~~obtained. The~~ then generated. A comparative analysis ~~of superimposed flooded~~with observed inundation points data shows a strong spatial alignment between the distribution of flooded points ~~in the study area~~ and the high to medium-high risk ~~areas~~zones, highlighting the reliability and applicability of the proposed model. The remainder of this paper is structured as follows: Section 2 describes the study area, data sources, and methodology; Section 3 presents the results and analysis; Section 4 discusses the findings and their implications; and Section 5 concludes the study with key insights and recommendations.

2 Materials and methods

In this section, the study area is briefly introduced (Section 2.1), and each individual component of the study is further discussed along with the basic geographic information, meteorology, social statistics, historical disaster data, and other fields involved in the study of urban agglomeration flood disasters and their risks (Section 2.2). The framework of the flood risk assessment model is shown in **Figure 1**. The factors influencing flood risk in the YRDUA are explored, and a flood risk assessment index system is established (Section 2.3). The optimal model in AutoML is selected to calculate the importance of flood hazard and hazard characteristic factors (Section 2.4), and the model is combined with AHP to determine the weight of each risk indicator (Section 2.5). Ultimately, a flood risk assessment model based on AutoML and AHP is constructed.

172
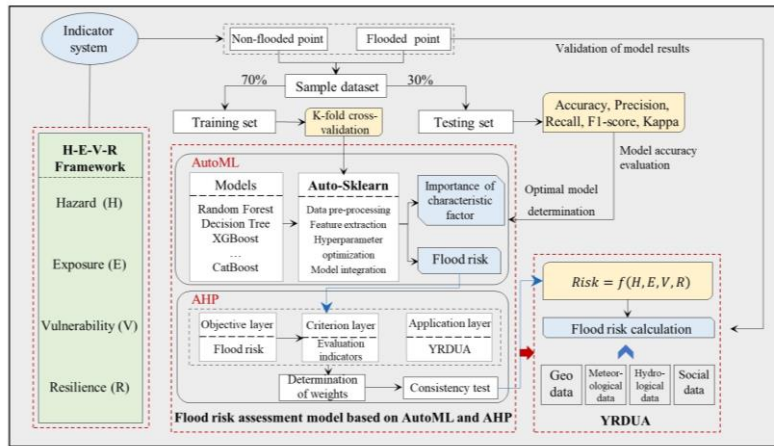
173 **Figure 1: Flood risk assessment modeling framework.**

174

2.1 Study area

176 The Yangtze River Delta Urban Agglomeration, located in the eastern coastal region of China (27° 04′–

177 34° 49′ N; 115° 75′–122° 95′ E), includes 27 cities: 8 in Anhui Province, 9 in Jiangsu Province, 9 in

178 Zhejiang Province, and Shanghai (**Figure 2**) (Yang et al., 2024). Influenced by the East Asian summer

179 monsoon, the study area features low-lying plains in the northern region and higher hilly terrain in the

180 southern region, along with numerous waterways (Ding et al., 2021). With the recent accelerated climate

181 change and urbanization, extreme precipitation events in the Yangtze River Delta (YRD) have been

182 occurring ever more frequently, and the temporal and spatial distribution differences in precipitation have

183 increased. Additionally, the increase in impervious surfaces, narrow plains rivers, and poor drainage may

184 result in more frequent and widespread urban flooding and waterlogging disasters (Wan et al., 2013).

185 This region is economically developed and densely populated , making it the largest urban agglomeration

186 in Asia (Sun et al., 2023). In 2008, the Gross Domestic Product (GDP) of the YRD accounted for 17.5%

187 of the GDP of the entire country, i.e., 4.3 trillion yuan, and the per capita GDP was 44,468 yuan, i.e.,

188 twice the national average level. The population has reached 97.2 million, i.e., 7.3% of China's total

189 population, and the region's average population density is 877 persons/km^2, i.e., approximately twice the

190 national average (Gu et al., 2011). Therefore, the potential risks of flood and waterlogging disasters are

191 substantial.

192

193
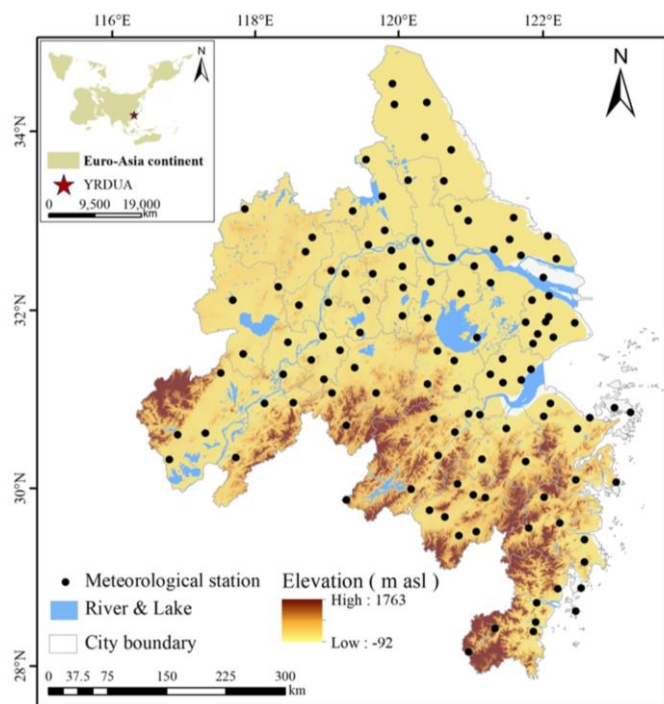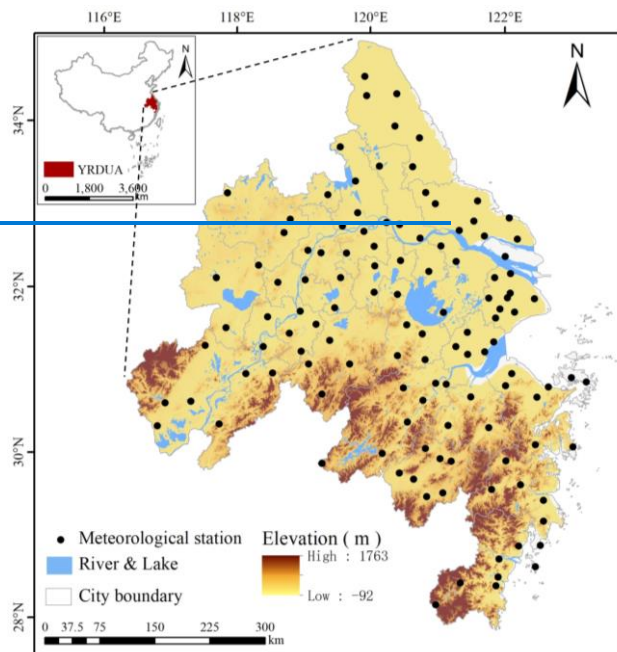
194 **Figure 2: The schematic map of the YRDUA.**

195

196 **2.2 Data sources and Processing**

197 **2.2.1 Data sources**

198 The study of flood disasters and their associated risks in urban agglomerations involves complex natural

199 and socio-economic factors. Therefore, we collected and preprocessed data from multiple fields, such as

200 basic geography, meteorology, social statistics, and historical disasters. **Table 1** lists the data types and

201 resolutions collected for the research area.

202 **Table 1: Description of the Datasets Used for Flood Risk Assessment, Their Characteristics, and Data Sources.**

Category	Details	Resolution	Data Source
Basic Geographic Information Data	Administrative boundaries and river network density data.	30m	-Resources and Environmental Science and Data Center, CAS (https://www.resdc.cn/). -USGS (https://earthexplorer.usgs.gov/). -Wuhan University CLCD dataset (https://zenodo.org/records/8176941). - National Ecosystem Science Data Center (nesdc.org.cn).
	Digital Elevation Model (DEM) based on SRTM1 (30m), mosaicked and clipped to the study area (27 core cities).		
	Land use data from CLCD (30m), includes 7 types: farmland, forest, shrubland, grassland, water, bare land, and impervious surfaces.		
	NDVI data (2000–2020) calculated using the GEE platform.		
Meteorological Data	Hourly precipitation data from 120 meteorological stations. Data preprocessed for outlier removal and missing value handling.	Station data	National Meteorological Information Center, China Meteorological Administration
Social Statistics	Population, unemployment, GDP, and healthcare statistics at the prefecture level.	Prefecture-level	Provincial and municipal statistical yearbooks and bulletins
	Urbanization rate calculated using urban population proportion.		
	GDP density and per capita GDP derived from total GDP and land area/population.		

	Flood inundation data from the MODIS-based Global Flood Database (2000–2018), processed to focus on the YRDUA region. To ensure comprehensive selection of inundation points, the inundated areas within the time frame were overlaid to produce a historical flood map.		
Historical Disaster Data		250m	Global Flood Database (https://www.emdat.be/).

203

2.2.2 Data Standardization and Preprocessing

Due to variations in data sources and formats, the collected flood disaster risk data exhibit differences in spatial resolution, dimensions, and magnitude. To ensure consistency and comparability, standardization of both spatial scale and numerical range was performed before using these datasets as flood risk indicators.

(1) Unification of spatial scale means aligning data within the same coordinate range and resolution. The research data is standardized through projection transformation, converting all datasets into the same geographic and projected coordinate systems. To generate continuous spatial surfaces from discrete data points, we applied the Ordinary Kriging interpolation method, which assumes a constant but unknown local mean (Cressie, 1990). A spherical semivariogram model was adopted to capture spatial autocorrelation, as it is widely used in environmental geostatistics for its bounded range and smooth continuity (Webster and Oliver, 2007)The Kriging interpolation method is used to spatially process all discrete data.. The interpolation process was carried out using ArcGIS 10.8. Finally, if the spatial data has different resolutions, resampling is performed to standardize all data to the same resolution, which in this study is unified to 30m×30m.

(2) Normalization of the numerical range can be achieved using a normalization process. Through a linear transformation, the values of the data are mapped to the range [0, 1], thus eliminating the influence of differing dimensions among the data indicators. In this study, the Min-Max Normalization method is used for normalization, and theIn this study, the Min-Max normalization method is applied. Specifically, the minimum and maximum values of each feature are computed only from the training set, and both the training and test sets are then normalized using these training-derived parameters. This ensures that the normalized values in the training set are scaled to the range [0,1], while the values in the test set may exceed this range if they fall outside the training set's value distribution. The formula is as follows:

227 $$x' = \frac{x - \min(x)}{\max(x) - \min(x)} \frac{x - x_{min}^{train}}{x_{max}^{train} - x_{min}^{train}}$$ (1)

228 **2.3 Establishment of an flood risk assessment indicator system**

229 **2.3 Historical Flood Inundation Point Extraction**

230 The historical flood inundation map of the study area is shown in **Figure 3**Figure 3 (a). The flood

231 inventory map used in this study was created based on inundation data from the Global Flood Database

232 and the EM-DAT flood disaster database, and further verified through satellite imagery, Google Earth,

233 and existingdocumented historical flood records. The actual flooded areas were delineated from flood

234 traces in the inundation dataset and image interpretation. DuringA flooded point is defined as a location

235 that lies within the inundation extent of at least one recorded flood event during the study period. Based

236 on this definition, 278 flooded points were randomly selected within the inundation data range. The

237 location of each point servesfrom the validated inundated areas. These points serve as the foundation for

238 subsequent statistical analysis of flood eventsand model training, with thetheir spatial distribution shown

239 in **Figure 3**Figure 3 (b).

240 To calculate flood hazard, it is necessary to select training samples. The task of identifying flooded and

241 non-flooded points using AutoML is essentially a binary classification problem, which requires a

242 balanced number of samples. An imbalanced ratio of positive and negative samples can result in

243 unreliable classification outcomes. Previous studies (Pham et al., 2021; Bostan et al., 2012) have shown

244 that the best classification performance is achieved when the ratio of flooded to non-flooded points is

245 1:1. Therefore, after selecting the flooded points, 278 non-flooded points were randomly sampled to

246 ensure a balanced 1:1 ratio, excluding high-altitude areas, based on the region's actual characteristics.

247 Finally, the flooded and non-flooded points were used as sample data and divided into a 7:3 ratio (70%

248 for training and 30% for testing) for model training.

249
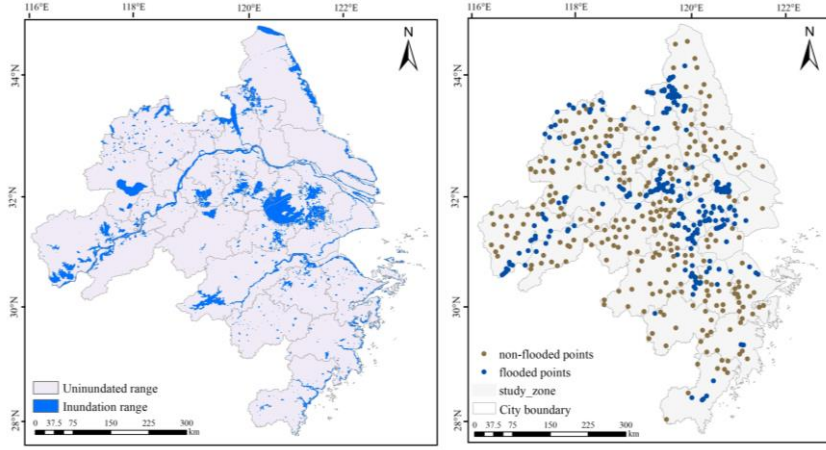
250 **Figure 3~~3~~: (a) Flood inundation map of the study area. (b) Spatial Distribution of Flooded and Non-Flooded**
251 **Points in the YRDUA.**

252

253

254 **2.4 Establishment of an flood risk assessment indicator system**

255 Although risk is a universal concept, it has no universal definition (Aven, 2016; Mishra and Sinha, 2020).

256 Based on the hazard–exposure–vulnerability (H–E–V) disaster risk framework, we considered the

257 particularity of flood risk research at the urban agglomeration scale, incorporated resilience indicators

258 into the existing framework, and constructed a four-dimensional flood risk assessment framework of

259 hazard–exposure–vulnerability–resilience (H–E–V–R) that can assess regional flood risks more

260 comprehensively and systematically. The conceptual description of flood risk in this study can be

261 expressed in the Eq. (2):

262 $Risk = f(H, E, V, R) = \sum_{i=1}^{a} \omega_H H_i + \sum_{i=1}^{b} \omega_E E_i + \sum_{i=1}^{c} \omega_V V_i + \sum_{i=1}^{d} \omega_R R_i,$ (2)

263 where H, E, V, and R represent the danger of, exposure to, vulnerability to, and resilience in response

264 to floods, respectively; ω_H, ω_E, ω_V, and ω_R are the weights of danger, exposure, vulnerability, and

265 resilience, respectively; H_i, E_i, V_i, and R_i are the values of items i of the indicators, respectively; and

266 a, b, c, and d are the numbers of the indicators, respectively.

267 We constructed a flood risk assessment index system for the YRDUA based on the "H–E–V–R"

268 framework, the actual situation of the study area, the formation mechanisms of flood disasters, and the

269 findings of relevant studies (Gain et al., 2015; Criado et al., 2019; Hsiao et al., 2021). We selected four

270 first-level indicators (i.e., hazard, exposure, vulnerability, and resilience indices) and 19 second-level

271 indicators. A detailed description of the flood risk assessment index system is presented in **Figure 4**.
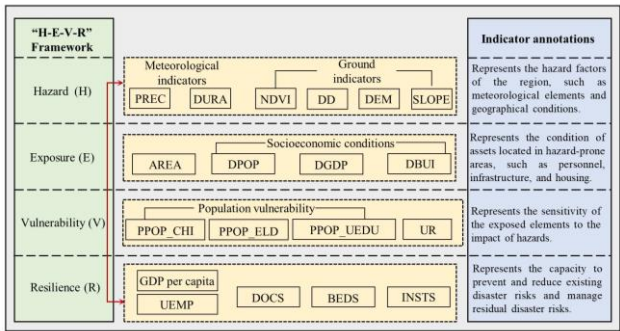
272 **Figure 4: Flood risk assessment index system for the YRDUA based on the H–E–V–R framework.**

273

274 The hazard indicators consisted of six indices: Average annual precipitation (PREC), Annual Cumulative

275 Heavy Rainfall Duration (DURA), Digital Elevation Model (DEM), SLOPE, Drainage Density (DD),

276 and Normalized Difference Vegetation Index (NDVI). Rainfall is the primary factor leading to flooding,

277 particularly extreme rainstorms caused by climate change. According to the Meteorological Bureau's

278 definition, a heavy rainstorm event is characterized by rainfall of 50mm or more within 24 hours. DURA

279 is defined as the total number of days with heavy rainstorm events occurring at all meteorological stations

280 within the study area each year. The more days heavy rainstorms accumulate and the longer their

281 duration, the greater the likelihood of flooding and other disaster events. DEM and SLOPE are important

282 topographical indicators. Areas with low DEM and SLOPE values are generally more susceptible to

283 flood threats. DD refers to the area of rivers or lakes per unit of land surface area and is a crucial indicator

284 of a watershed's structural characteristics. It determines the watershed's capacity to withstand flooding.

285 The higher the DD, the greater the likelihood of flooding and the higher the potential flood risk.

286 Vegetation plays a role in water storage, retention, and infiltration. The lower the vegetation coverage,

287 the weaker the buffering capacity, making it more likely for surface water to accumulate. The NDVI

288   index measures the relative abundance of green vegetation, with values ranging from -1 to 1. The higher

289   the value, the greater the vegetation coverage, and the lower the risk of flooding.

290   Land area (AREA), Population Density (DPOP), GDP Density (DGDP), and Building Density (DBUI)

291   were selected as exposure indicators to assess the degree of vulnerability of both the natural environment

292   and social systems to flooding. The land area for each administrative unit at the prefecture-level city is

293   calculated individually. A larger land area corresponds to a greater extent exposed to flooding. DPOP

294   and DGDP represent the concentration of population and assets, respectively. Areas with higher DPOP

295   and DGDP are more susceptible to potential threats from pluvial flooding. DBUI, the ratio of total

296   building area to total land area in a region, indicates the building density. A higher DBUI reflects greater

297   exposure to flooding.

298   Vulnerability indicators focus more on the social aspects of flood disasters. This study selects four

299   vulnerability indicators: Proportion of Child Population (PPOP_CHI), Proportion of Elderly Population

300   (PPOP_ELD), Proportion of Uneducated Population (PPOP_UEDU), and Urbanization Rate (UR). Age

301   is a key feature of social vulnerability, and both the population aged 0-14 and those over 65 are considered

302   vulnerable groups, as these age groups are more susceptible to flood damage. The uneducated population

303   generally has a weaker awareness of disaster risks and lower self-protection capacity, which makes this

304   group more vulnerable to flooding. The urbanization rate refers to the proportion of the urban population

305   in the total resident population of a region. This indicator is inversely related to flood vulnerability. In

306   general, a higher urbanization rate indicates greater social development and stronger protective

307   capacities, which can reduce vulnerability to flooding to some extent.

308   The resilience indicators selected in this study include Gross Domestic Product (GDP) per capita,

309   Unemployment Rate (UEMP), Number of Doctors (DOCS), Number of Medical Institutions (INSTS),

310   and Number of Hospital Beds (BEDS). GDP per capita is the ratio of a region's GDP to its total resident

311   population over a specified period, reflecting the region's economic condition. A higher GDP per capita

312   indicates a more developed economy, which is associated with a greater capacity to recover quickly after

313   a flooding event. The Unemployment Rate (UEMP) measures the proportion of the idle labor force,

314   indirectly reflecting the stability of urban development. A high unemployment rate signals economic

315   instability, which weakens the capacity to cope with floods and extends the time required for post-disaster

316   recovery, thus impeding disaster response efforts. The indicators of DOCS, INSTS, and BEDS provide

317 insights into a region's healthcare and medical support capabilities. Areas with stronger healthcare
318 systems are better positioned to manage flood risks and recover more effectively from such disasters.
319

2.5 Flood risk calculation method based on AutoML

2.5.1 Feature selection

The flood inventory map in this paper was developed using inundation data from the Global Flood Database and flood disaster data from the EM-DAT database, supplemented by satellite and Google image interpretation and verified against existing historical flood records. The actual flood-affected areas were delineated based on flood traces from the inundation datasets and image interpretations. For this study, 278 flood inundation points were randomly selected within the inundation data range during the study period, and the location of each point was used as the basis for subsequent statistical analysis of flood events. The main factors affecting flood risk were considered during input feature selection. Rainfall and rainstorms are important factors that lead to floods, and flooding is closely related to topography, slope, vegetation cover, and hydrological conditions. Therefore, six indicator factors, namely PREC, DURA, DEM, SLOPE, NDVI, and DD, were selected as the input features of the model. To verify the model, 70% of the data in the sample were set as the training dataset and the remaining 30% of the data were set as the testing dataset through random sampling.

When the number of samples is small, data balancing is essential to ensure uniform sampling and reduce the deviations among the training, validation, and original datasets. Data balancing refers to the process of achieving a balanced distribution of data for each labeled category; it is particularly important when the number of observations in each class is significantly different. One way to address an imbalanced dataset is to oversample the minority classes. In this study, we assessed flood risk based on the identification of flooded point in the sample, which is essentially a binary classification problem; therefore, the output features are 0, i.e., negative categories (non-flooded points), versus 1, i.e., positive categories (flooded points). The processed dataset comprised 278 positive samples (flooded points) and 278 negative samples (non-flooded points), with each label consisting of 278 points representing the entire dataset.

2.5.2 Model training and hyperparameter optimization

Training samples were generated using the data from flooded and non-flooded points in the study area, and the Auto-Sklearn was used for model training, its principle is shown in **Figure 5**. The Auto-sklearn framework has multiple built-in machine learning algorithms. We selected 9 models that are more typical or have better performance in flood hazard research: random forest (RF), extreme gradient boosting (XGBoost), Light Gradient Boosting Machine (LightGBM), categorical feature boosting (CatBoost), Extra trees, Decision tree, Nearest Neighbors, Multi-layer Perceptron (MLP) neural network, and Linear Regression. The training and testing datasets were used to train the 9 machine learning models, and the hyperparameters were continuously adjusted and optimized.
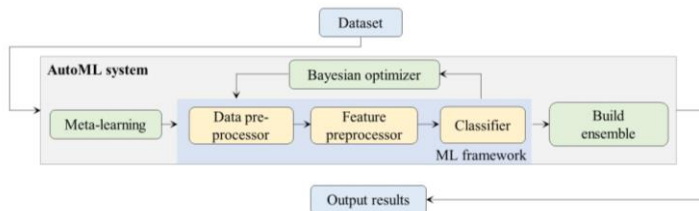
Figure 5: Principles of Auto-Sklearn

Hyperparameter optimization is an important step in ML model training. The aim of this step is to determine a hyperparameter combination to generate a ML model that performs well on a specific dataset and reduces the effect of the predefined loss function on a given dataset. In this study, we used a grid search strategy for optimization. For each set of hyperparameter combinations, k-fold cross-validation was used to evaluate the model and determine. To quantify the hyperparameter combination of the optimal model that achieved the best balance ofbetween Precision, and Recall, andthe F1-score was used as the primary evaluation metric. The hyperparameter combination corresponding to the model with the highest average F1-score was selected as optimal. Briefly, the training dataset was divided into K parts, of which one was selected as the test set and the rest were used as the training set. The cross-validation was repeated K times and the results were averaged K times. The model with the best average result among all models was selected as the optimal model, and the final classification prediction result was the output. In this study, we used 5-fold cross-validation.

368 It is important to note that 5-fold cross-validation was employed at two distinct stages in this study. First,

369 it was conducted within the training set during hyperparameter tuning as part of the AutoML model

370 selection process. Second, following final model selection, an independent 5-fold cross-validation was

371 applied to the entire dataset to evaluate the generalization performance of the model and identify potential

372 overfitting. The data partitions used in the two stages were entirely separate, ensuring that no data leakage

373 occurred.

374 **2.5.3 Performance evaluation**

375 To better compare the performance of the 9 selected ML models in the Auto-Sklearn framework for flood

376 risk assessment, multiple evaluation indicators were used to assess the test dataset. The following

377 combinations of the true category of the sample point and the category predicted by the classifier were

378 used: True Positive (TP)—the sample point is a flooded point, and the model classifier also predicts that

379 it is a flooded point; True Negative (TN)—the sample point is a non-flooded point, and the model

380 classifier also predicts that it is a non-flooded point; False Positive (FP)—the sample point is a non-

381 flooded point, and the model classifier mistakenly predicts that it is a flooded point; False Negative

382 (FN)—the sample point is a flooded point, and the model classifier mistakenly predicts that it is a non-

383 flooded point. Therefore, four related indicators were selected: Precision, Recall and F1-score, and the

384 consistency metric Kappa coefficient. The calculation formulas are as follows:

385 $$Precision = \frac{TP}{TP+FP} \ , \tag{3}$$

386 $$Recall = \frac{TP}{TP+FN} \ , \tag{4}$$

387 $$F1-_{score} = \frac{2TP}{2TP+FP+FN} \ , \tag{5}$$

388 Among the indicators, *Precision* refers to the proportion of correctly predicted flooded points among all

389 predicted flooded points, reflecting the model's ability to avoid false positives. *Recall* measures the

390 proportion of correctly identified flooded points among all actual flooded points, representing the

391 model's sensitivity. *F1-score* is the harmonic mean of Precision and Recall, providing a balanced

392 evaluation of both metrics and reflecting the overall recognition performance of the model.

393 *Kappa* coefficient is a statistical consistency metric used to measure classification performance, which

394 is calculated based on the confusion matrix of true and predicted categories. Its value ranges from [-1,1]:

395 A Kappa value of 1 indicates perfect agreement, 0 means the classification is no better than random

396 guessing, and negative values suggest the classification is worse than random prediction. *Kappa* is

397 calculated using Eq. (6), where P_e is given by Eq. (7).

398 $Kappa = \frac{P_o - P_e}{1 - P_e}$, $\qquad\qquad\qquad\qquad\qquad\qquad\qquad\qquad\qquad$ (6)

399 $P_e = \frac{(TP+FP)(TP+FN)+(TN+FN)(TN+FP)}{(TP+FP+TN+FN)^2}$, $\qquad\qquad\qquad\qquad\qquad\qquad$ (7)

400 where P_e represents the expected agreement by chance.

401 Combining multiple indicators allows for a more comprehensive evaluation of models within the Auto-

402 Sklearn framework for flood point identification and flood risk assessment.

403 **2.6 Method for determining flood risk index weights based on AHP**

404 **2.6.1 Establishing a hierarchical model**

405 According to the decision-making objectives, factors, and applications in decision-making problems, the

406 AHP can be divided from bottom to top into the target, criterion, and application layers. Among them,

407 the target layer is the problem to be solved (i.e., final flood risk). The criterion layer is the intermediate

408 link, including the factors to be considered and the decision making criteria. The factors can be divided

409 into different evaluation indicators, including four first-level indicators (danger, exposure, vulnerability,

410 and resilience) and their corresponding 19 second-level indicators. The criterion layer comprises various

411 weight combination schemes linked to the target layer. The application layer is the final optional scheme

412 and specific application of the decision. The final weight scheme and evaluation results of this study

413 were applied to the YRDUA.

414 **2.6.2 Constructing the judgment matrix**

415 After the hierarchical structure was established, a judgment matrix was constructed based on the

416 relationship between the criteria and indicators. Different elements in the sublevel were compared

417 pairwise, and the relative importances of all elements in the current layer and previous layer were

418 compared. Typically, a pairwise comparison matrix is used as representative. In this study, we adopted

419 the 1–9 scale method as the importance measurement standard. The importance comparison relationship

420 is presented in **Table 2**, where the matrix element a_{ij} represents the comparison result of the ith element

421 relative to the jth element.

422 **Table 2: Pairwise comparison point-based rating scale of AHP.**

Ranking	Importance Level
1	Equally important
3	i is slightly more important than j
5	i is much more important than j
7	i is very much more important than j
9	i is extremely important than j
2, 4, 6, 8	Intermediate value of two adjacent judgments
Reciprocal	Comparative judgment of j vs., $a_{ji} = 1/a_{ij}$

423

2.6.3 Solving the eigenvector of the judgment matrix

425 Based on the judgment matrix, the square root method was used to solve the eigenvector and eigenroot.

426 The first step is to calculate the square root a_{ij} of the product of each row of the judgment matrix n,

427 then normalize it, and finally calculate the maximum eigenroot of the judgment matrix. The formula is

428 as Eq. (8), Eq. (9), Eq. (10).

429
$$M_i = \sqrt[n]{\prod_{j=1}^{n} a_{ij}}, \tag{8}$$

430
$$W_i = \frac{M_i}{\sum_{i=1}^{n} M_i}, \tag{9}$$

431
$$\lambda_{max} = \sum_{i=1}^{n} \frac{(AW)_i}{nW_i}, \tag{10}$$

2.6.4 Consistency check

433 After the eigenvector calculation is completed, a consistency test is required to reduce the subjectivity in

434 the judgment matrix and enhance the scientific nature of the data and calculations. In a pairwise

435 comparison matrix, consistency means that the decision-maker's judgments must exhibit logical

436 coherence and transitivity. Specifically, if option A is considered more important than option B, and

437 option B is considered more important than option C, then consistency requires that option A must also

438 be judged more important than option C (Saaty, 1984).

439   The consistency indicator (CI) is used to measure the deviation of the judgment matrix from the

440   consistency: the smaller the CI, the greater the consistency of the judgment matrix. When CI = 0, the

441   judgment matrix is completely consistent. The CI calculation formula is as Eq. (11).

442    $CI = \frac{\lambda_{max} - n}{n - 1}$,   (11)

443   To quantify the standard, the relative consistency (CR) index was further calculated as Eq. (12).

444    $CR = \frac{CI}{RI}$,   (12)

445   Where average Random Consistency Index (RI) represents the average random consistency which

446   depends only on the order of the judgment matrix. The RI values for judgment matrices of order 1 to 10

447   are shown in **Table 3**.

448   **Table 3: Consistency index (RI) for a randomly generated matrix.**

n	1	2	3	4	5	6	7	8	9	10
RI	0.00	0.00	0.52	0.89	1.12	1.26	1.36	1.41	1.46	1.49

449

450   CR was determined based on the RI value. When CR < 0.1, the consistency of the judgment matrix is

451   considered good. When CR > 0.1, the consistency of the judgment matrix is unacceptable, and the

452   judgment matrix must be adjusted and modified. In such cases, the corresponding judgment matrix was

453   further constructed, and the eigenvector and eigenroot were calculated using the following formulas:

454   Finally, the judgment matrix that passed the consistency test was used to calculate the weights of the

455   indicators at the different levels.

456   **2.7 Determination of flood risk levels**

457   The classification of flood risk levels often involves manually setting thresholds, which can introduce

458   subjectivity and influence the accuracy of the risk assessment outcomes (Ma et al., 2022). To calculate

459   the flood risk, we employed the natural breakpoint classification method, which groups data into classes

460   based on natural divisions within the dataset (Lin et al., 2019). This method works by identifying points

461   where the data distribution changes most significantly and dividing the data into ranges based on these

462   breaks. Unlike clustering methods, which do not focus on the number and range of elements in each

463   group, the natural breakpoint method ensures that the range and number of elements in each group are as

464   balanced as possible (Ma et al., 2022).

3 Results and discussion

3.1 Model flood risk results and evaluation

3.1.1 AutoML optimal model selection

In the experiment, 9 typical ML models under the Auto-Sklearn framework were used to process the sample dataset, with 70% of the sample set being used as the training dataset and 30% being used as the testing dataset. The results of the comparative analysis of the model performance based on the test dataset are presented in **Table 4**. A comprehensive analysis of the results on the testing data revealed that, in terms of Precision, CatBoost had the highest value (0.9030), followed by LightGBM (0.8960) and Extra Trees (0.8893). Meanwhile, CatBoost had the highest recall rate of 0.8883, followed by that of Extra Trees at 0.8870. The probability thresholds for Precision, Recall, and F1-score range from [0,1], while the Kappa coefficient ranges from [-1,1]. The F1-score and Kappa coefficient of the CatBoost model were also markedly higher than those of the other models, reflecting the model's good consistency. A comprehensive comparison showed that the precision, F1-score, and Kappa coefficient of the CatBoost model were the highest, with its precision reaching 0.9030, indicating that the recognition and prediction precision of the flooded points in the study area based on the CatBoost model were obviously better than those of other common machine learning models.

Since flood data often involve various environmental factors and complex interactions, the CatBoost model is highly effective at handling these ~~intricate~~ nonlinear relationships and feature interactions. Additionally, the model incorporates multiple regularization mechanisms during tree construction, which helps ~~prevent~~reduce overfitting and enhances the model's generalization capability. As shown in **Table 4**~~The results indicate that,~~ most models performed well on the training set, but their performance slightly declined on the test set, highlighting variations in generalization ability. CatBoost demonstrated strong robustness, achieving a Precision of 0.9319 on the training set and 0.9030 on the test set. Additionally, LightGBM and XGBoost showed relatively consistent performance between the training and test sets, suggesting better generalization. However, models such as Decision Tree and Nearest Neighbors exhibited a more significant performance drop in the test set, indicating a higher sensitivity to overfitting. Interestingly, in a few cases (e.g., Extra Trees), test set performance slightly exceeded that of the training set in certain metrics. This is not uncommon in small, balanced datasets and may result from a combination of factors such as random sampling variation, slightly easier test samples, or appropriate

494 regularization that reduces overfitting in the training set. To further evaluate overfitting, we used 5-fold
495 cross-validation by comparing the performance of the training and testing sets. The experimental results
496 indicate that while most models showed some performance decline on the test set, CatBoost maintained
497 relatively stable performance, suggesting that the model does not exhibit significant overfitting and has
498 good generalization ability.

499 **Table 4: Comparative analysis of the performances of different ML models.**

Models	Dataset	Precision	Recall	F1-score	Kappa
CatBoost	Training set	0.9319	0.9307	0.9547	0.8614
	Testing set	0.9030	0.8883	0.8960	0.7915
XGBoost	Training set	0.9017	0.8827	0.8818	0.8640
	Testing set	0.8748	0.8640	0.8624	0.7256
LightGBM	Training set	0.9349	0.9307	0.9306	0.8616
	Testing set	0.8960	0.7890	0.8015	0.7324
Random Forest	Training set	0.8922	0.8747	0.8745	0.7484
	Testing set	0.8482	0.8320	0.8309	0.6662
Extra Trees	Training set	0.8524	0.8240	0.8735	0.7695
	Testing set	0.8893	0.8570	0.8877	0.7751
Decision Tree	Training set	0.8886	0.8640	0.8621	0.8040
	Testing set	0.8810	0.8720	0.8708	0.7419
Linear Regression	Training set	0.8636	0.8533	0.8525	0.7073
	Testing set	0.8682	0.8480	0.8450	0.6926
Nearest Neighbors	Training set	0.7301	0.7907	0.7987	0.6009
	Testing set	0.7747	0.7440	0.7390	0.4937
MLP Neural Network	Training set	0.8998	0.8880	0.8873	0.7765
	Testing set	0.8682	0.8480	0.8450	0.6926

500

501 By comparing the performances of the 9 models, we found that the CatBoost model was more effective
502 in identifying flooded points. To further verify the excellent performance of the model, the receiver
503 operating characteristic (ROC) curve and area enclosed by the coordinate axes (corresponding area under
504 the curve [AUC] value) were plotted based on the test dataset to assess the model's binary classification
505 effectiveness: the larger the AUC value, the better the model distinguishes between classes. When AUC
506 > 0.8, the model prediction effect is very good (Sinha et al., 2008). In this study, both micro- and macro-

507 average ROC curves were plotted. The micro-average ROC curve aggregates the contributions of all

508 classes to compute the average ROC curve, treating each instance equally, while the macro-average ROC

509 curve computes the ROC curve for each class independently and then averages the results. These two

510 methods are commonly used for multi-class classification problems, but in this study, they were used to

511 give a more comprehensive comparison of model performance. The verification results are shown in

512 **Figure 6**. The AUC value of the CatBoost model reached 0.91, guaranteeing the performance and

513 prediction reliability of the CatBoost model. Based on this, the CatBoost model was selected to calculate

514 the flood risk in the YRDUA.

515
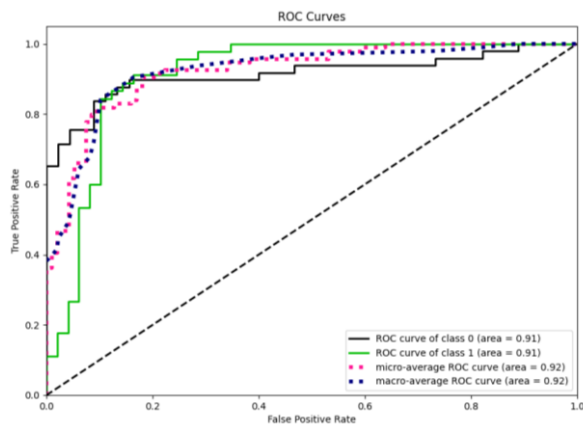
516 **Figure 6: Receiver operating characteristic (ROC) curves and corresponding area under the curve (AUC)**

517 **values of the CatBoost model.**

518

519 **3.1.2 Importance and Interpretability Analysis of Hazard Factors**

520 In this study, the AutoML model was used specifically to assess flood hazard, which represents the

521 physical likelihood of flood occurrence and is directly driven by environmental factors such as rainfall,

522 topography, and drainage characteristics. Therefore, only the six second-level indicators under the hazard

523 dimension were used as input features in the AutoML model. This approach allowed us to focus the

524 model on identifying the key natural drivers of flooding, while the other dimensions — exposure,

525 vulnerability, and resilience—were later incorporated via the AHP method for comprehensive flood risk

526 evaluation.

527 To better understand the contribution of different hazard indicators to flood risk in the YRDUA, we

528 conducted both importance ranking analysis using the CatBoost model and interpretability analysis based

529 on SHAP.

530 The CatBoost model was used to quantify the relative importance of six key hazard indicators. The results,

531 shown in **Figure 7**, reveal significant differences in their influence. DEM was identified as the most

532 critical factor, contributing 68.55%, which far exceeds the other factors, which is also in line with the

533 findings of many researchers within the region (Mei et al., 2021; Wan et al., 2013). Low-lying areas

534 naturally function as water accumulation zones, increasing flood vulnerability. Additionally, urban areas

535 in the YRDUA are dominated by impervious surfaces, limiting infiltration and exacerbating flood risks.

536 While PREC is a primary factor in storm-induced flooding, its direct contribution to flood risk was

537 relatively low compared to DURA, which accounted for 10.07%. This highlights that the persistence of

538 extreme rainfall events is a stronger predictor of flood hazard than total annual precipitation.
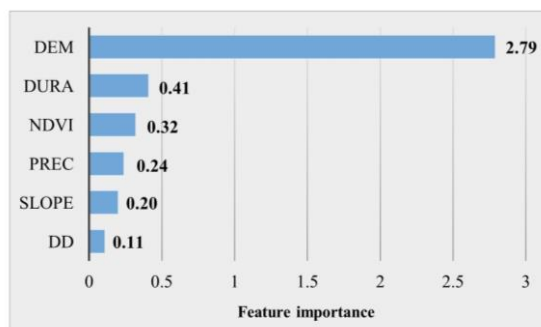
539
540 **Figure 7: Importance Ranking of Hazard Factors Based on the CatBoost Model**

541

542 To further analyze the interpretability of the model and understand the impact of individual flood hazard

543 indicators on the model's classification results, this paper calculates Shapley Additive Explanations

544 (SHAP) to indicate the contribution of each feature in the sample (Lundberg and Lee, 2017). SHAP, a

545 game theory-based post-hoc interpretation method, quantifies the marginal impact of each feature on

546 model predictions. The SHAP summary plot in **Figure 8** (a) ranks features based on their absolute SHAP

547 values, consistent with the CatBoost importance ranking. Each row represents a feature, where red

548 indicates higher feature values and blue indicates lower values. The results show that DEM, SLOPE, and

549 NDVI negatively impact flood risk, meaning that higher elevation, steeper slopes, and greater vegetation

550 coverage reduce flood hazards. In contrast, DD, DURA, and PREC positively impact flood risk,

551 indicating that higher drainage density, longer durations of extreme rainfall, and increased precipitation

552 levels contribute to higher flood hazards. Among these, DEM has the highest absolute SHAP value, with

553 a strong clustering below zero, reinforcing its dominant role in flood risk determination.
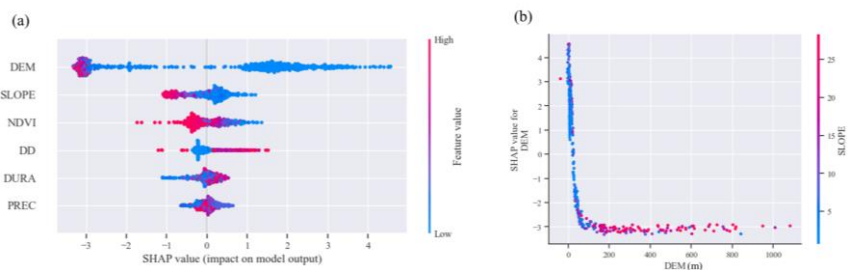
554
555 **Figure 8: (a) Scatter Plot of Hazard Indicators from SHAP Analysis. (b) SHAP Dual Dependence Analysis of**
556 **Elevation and Slope Factors.**

557

558 To directly capture the interaction effects between paired indicator factors, this study used SHAP

559 interaction values based on game theory, ensuring consistency while also explaining the interaction

560 effects of individual predictions. For the DEM feature, which had the highest importance in the SHAP

561 analysis, the factor most strongly correlated with it was SLOPE. Therefore, to illustrate how one feature

562 interacts with another to affect the model training results, this study used DEM and SLOPE as examples

563 to plot the SHAP interaction scatter plot, representing the dependency of the DEM feature. The results

564 are shown in **Figure 8** (b). This dependency plot takes the form of a logarithmic function, indicating that

565 as DEM increases, the flood hazard decreases. Additionally, the slope has a negative effect on the flood

566 hazard in relation to elevation; that is, at lower elevations and gentler slopes, the flood hazard is greater.

567 **3.1.3 Determination of flood risk index weights**

568 A judgment matrix was constructed for 19 indicator factors. A hazard index was constructed based on

569 feature importance calculated using AutoML. The exposure, vulnerability, and resilience indicators were

570 determined based on existing literature and relevant expert scores (Hsiao et al., 2021). ~~Combined with~~

571 ~~the actual characteristics of the YRDUA, the 1–9 scale method was used to compare item by item any~~

572 ~~two indicators and determine their relative importances and assign weights.~~. The judgment matrices were

573 constructed using a hybrid approach. For the hazard indicators, feature importance scores generated from

574 the AutoML model were used to inform the pairwise comparisons. For the exposure, vulnerability, and

575 resilience indicators, the weights were determined by the authors based on a combination of expert

576 judgments, a review of existing studies, and consideration of the local conditions in the YRDUA. The

577 Saaty 1–9 scale was applied to assign relative importance to each pair of indicators. Finally, the judgment

578 matrix results were tested for consistency, and the CR value was 0.0058, i.e., $\ll$ 0.100, indicating that

579 the results passed the consistency test and that the flood risk index weight values calculated using the

580 AHP were acceptable. The specific indicator weights and their corresponding impacts on flood risk are

581 shown in Table 5. The "Attribute" column represents the impact of each indicator on flood risk, with "+"

582 indicating a positive impact on flood risk and "-" indicating a negative impact on flood risk.

583 **Table 5: Flood risk index weights.**

Dimension	Indicator	Unit	Attribute	Weight
Hazard (0.4798)	PREC	mm	+	4%
	DURA	Day	+	10.8%
	NDVI		-	7.6%
	DEM	km	-	22.99%
	SLOPE	°	-	6.4%

Dimension	Indicator	Unit	Attribute	Weight
Exposure (0.1083)	DD	km/km^2	+	3.2%
	AREA	km^2	+	1.1%
	DPOP	people/km²	+	4.32%
	DGDP	10,000 yuan/km²	+	3.84%
	DBUI	km^2	+	1.16%
Vulnerability (0.1312)	PPOP_CHI	%	+	4.92%
	PPOP_ELD	%	+	3.04%
	PPOP_UEDU	%	+	2.11%
	UR	%	-	2.05%
Resilience (0.2807)	GDP per capita	100 million yuan/10,000 People	-	4.43%
	UEMP	%	+	5.04%
	DOCS	Per person	-	4.13%
	INSTS	Each	-	0.45%
	BEDS	Per bed	-	6.28%

584

585 The weighted results reflect the degrees of influence of the different indicator factors on flood risk.

586 Danger was the decisive factor affecting flood risk, with a weight of 0.4798, followed by resilience and

587 vulnerability. Exposure had a relatively low impact on flood risk. In terms of danger, the topography and

588 DURA were the main factors affecting the occurrence of flooding. These two indicators determined the

589 characteristics of flood disasters in the YRDUA from the perspective of disaster-prone environments and

590 driving factors, respectively. In terms of exposure, the YRDUA is a typical area with rapid social,

591 economic, and population growths in China. High population and GDP densities increase the risk of

592 flood exposure. In addition, the uneven age distribution and education levels of the population are

593 important social factors affecting the risk of flood disasters in urban agglomerations. In terms of

594 resilience, improving health and medical infrastructure, developing the regional economy, and reducing

595 unemployment rates are conducive to improving the overall disaster response capacity of the region and

596 reducing the risk of flood disasters in the YRDUA.

3.1.4 Model results verification

Based on CatBoost under the AutoML framework and AHP, the levels of flood hazard, exposure, vulnerability, and resilience were calculated for floods in the YRDUA and the spatial distribution of flood risks in the region was obtained according to the weights determined by the model. Combined with the natural breakpoint classification method, a flood risk zoning map of the YRDUA was constructed. The extracted flood points were superimposed on the map to verify whether the model exhibited good flood risk assessment capabilities. The results are shown in **Figure 9**, indicating that the distribution of flood points was consistent with the distribution of high and medium-to-high risk areas in the region, with the model assessment results corresponding well with the actual flooding situation. To specifically illustrate the correspondence of the results, the proportion of flood points distributed in high and medium-to-high risk areas was quantitatively calculated. The obtained value was 87.45%, indicating that the flood risk assessment results of the model in this study were highly credible, and subsequent analysis could be conducted.

As shown in **Figure 9**, the high and medium-to-high risk areas in the YRDUA were mainly located in the northern part of the region, concentrated in Chizhou, Anqing, Ma'anshan, and Xuancheng Cities in Anhui Province, Yancheng and Yangzhou Cities in Jiangsu Province, and Taizhou City in Zhejiang Province. Meanwhile, most areas of Hangzhou City had the lowest risk. The flood risks in cities such as Shanghai, Nanjing, and Jinhua were also relatively low. The overall analysis showed that the flood risk in the study area was low in the southwest and high in the northeast, determined largely by natural terrain and meteorological factors. The spatial distribution of the flood hazard class was similar to the distribution of flood risks; exposure decreased stepwise from Shanghai to the surrounding areas, reflecting that densely populated and economically developed cities have higher exposure. Areas with higher vulnerability were mainly concentrated in Chizhou, Anqing, Xuancheng, Chuzhou, and Yancheng Cities. The number of vulnerable people in these cities was relatively high. Vulnerability has aggravated the flood risks in Chizhou and Anqing Cities on the basis of flood risk. Meanwhile, Shanghai had the best resilience performance, followed by those of Hangzhou, Suzhou, and Nanjing Cities, greatly lessening the flood risks in these cities.

624
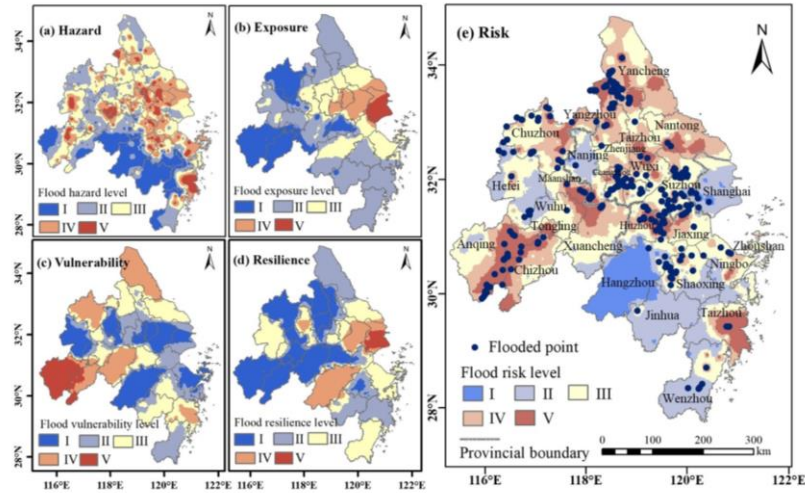
Figure 9: Flood risk level distribution and verification results based on a flood risk assessment model. The flood hazard, exposure, vulnerability, and resilience of the YRDUA were calculated using CatBoost under the AutoML framework and AHP. The flood hazard level (a), flood exposure level (b), flood vulnerability level (c), flood resilience level (d), and flood risk spatial distribution (e) were derived through natural breaks classification in ArcGIS software based on model-determined weights, resulting in a flood risk zoning map for the Yangtze River Delta region.

631

3.2 Analysis of changes in the spatiotemporal characteristics of flood risk

The flood risk results for the YRDUA from 1990 to 2020 were obtained based on the flood risk assessment model proposed in this study. The differences in flood risk among cities in the YRDUA over the past few decades are primarily due to a complex interplay of various factors, including geographic and climatic conditions, urbanization processes, socio-economic factors, ecological changes, and historical flood events. The topography and precipitation patterns of different cities affect their capacity for rainwater drainage and accumulation, while urbanization leads to an increase in impervious surfaces and variations in infrastructure development, impacting flood management capabilities. Additionally, differences in DPOP, economic development levels, and flood management policies can exacerbate flood risk. Furthermore, the increasing frequency of extreme weather events due to climate change further elevates flood risk. These factors determine the varying levels of flood risk among cities within the YRDUA.

644   As the interannual difference in flood risk in the region was small and the change response was weak,

645   we selected the flood risk results for 1990, 2000, 2010, and 2020 to analyze the changes in the

646   spatiotemporal pattern. In this analysis, variables such as PREC and DURA exhibit clear temporal

647   variability, as they change year by year due to weather patterns. However, other factors like DEM,

648   SLOPE, NDVI, and urbanization indicators such as DPOP and GDP are spatial variables that do not

649   exhibit direct temporal changes, but their effects on flood risk are influenced by changing socio-economic

650   and ecological conditions.

651   Regarding spatial patterns (**Figure 10**), the flood risk in the YRDUA showed clear spatial heterogeneity.

652   The southwestern part of the study area and Shanghai have shown low flood risks over the past 30 years,

653   whereas the central and northern parts of the region have been more likely to face flood risks depending

654   on the natural conditions, population, economic conditions, and recovery capacity of the region.

655   Regarding temporal patterns, from 1990 to 2010, areas with high and medium-to-high risk decreased

656   markedly. By 2010, most of the YRDUA (except for a few areas) was in a state of medium risk or below,

657   with the southwestern region exhibiting a large range of low risk levels. The corresponding areas for

658   each risk level are shown in **Figure 11**. From 1990 to 2010, areas of low and low-to-medium risk levels

659   gradually increased, maximizing in 2010, whereas areas of medium risk and above continued to decrease.

660   By 2020, the number of high-risk areas for flooding increased. There is a tendency for areas of medium-

661   to-high risk in the central region to shift towards high-risk areas in 2020, as compared to the state in

662   1990. Meanwhile, high-risk areas for floods also appeared in Chizhou and Anqing Cities in Anhui

663   Province, which was mainly due to the intensification of extreme weather, unbalanced population

664   distribution, and rapid economic development in recent years.

665
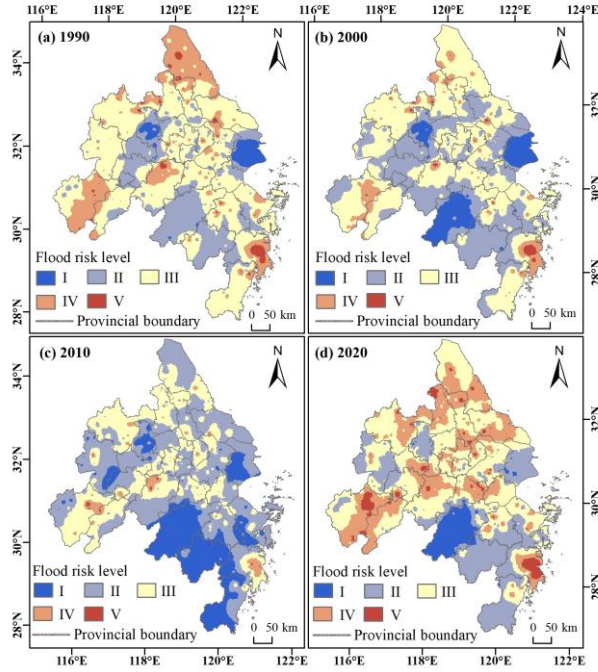
Figure 10: Spatial distributions of flood risk in the YRDUA in different years during 1990–2020.

667

668
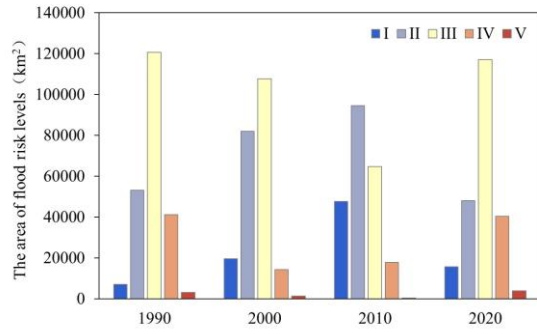
Figure 11: Areas at different levels of flood risk in the YRDUA in different years during 1990–2020.

670

671 To further analyze the changes in flood risk in the region, we calculated the change rate of the area of

672 different risk levels every 10 years and the overall change rate over 30 years. The interannual rate of

673 change was expressed in Eq. (13).

674 $\quad R_{l,ij} = \frac{Risk_{l,j} - Risk_{l,i}}{Risk_{l,i}} \times 100\%,$ (13)

675   where $R_{l,ij}$ is the rate of change of the flood risk area of a certain level l in a certain year, i and j are

676   different years, and $Risk_{l,j}$ and $Risk_{l,j}$ are the areas corresponding to the flood risk of this level in

677   different years.

678   The interannual variation rate of the flood risk is shown in **Table 6**. Results showed that the interannual

679   variation between the areas of low and high risk was relatively large. The low-risk area maximized in

680   2010, and both R $_{2000–1990}$ and R $_{2010–2000}$ showed a positive variation rate. The high-risk area showed the

681   largest interannual variation rate from 2010 to 2020, reaching 12.22% and causing the high-risk flood

682   area in 2020 to spread, resulting in a large high-risk area.

683   **Table 6: Interannual change rates of flood risk areas of different levels (expressed as percentages).**

	R$_{2000-1990}$	R$_{2010-2000}$	R$_{2020-2010}$	R$_{2020-1990}$
I	1.77%	1.44%	-0.67%	1.21%
II	0.54%	0.15%	-0.49%	-0.10%
III	-0.11%	-0.40%	0.81%	-0.03%
IV	-0.65%	0.25%	1.25%	-0.02%
V	-0.53%	-0.80%	12.22%	0.27%

684

685   Analyzing the flood risk of the entire urban agglomeration does not reveal the spatial scale effect of flood

686   risk, nor does it consider the correlation and impact of flood risk at different spatial scales. To reflect the

687   distribution of and changes in flood risk at different spatial scales within the region, the risk intensity of

688   different provinces was further analyzed, and the results are shown in **Figure 12**, respectively. In **Figure**

689   **12**, the average flood risk reflects the differences in risk development of the provincial administrative

690   units in Shanghai, Anhui, Zhejiang, and Jiangsu in terms of time and space. Overall, all administrative

691   units in the YRDUA exhibited the highest flood risk in 2020, and the overall risk trend increased. At the

692   provincial level, Shanghai's flood risk was consistently low, showing a trend of first decreasing from

693   0.152 in 1990 to 0.123 in 2000 and then gradually increasing to 0.311 in 2020. Among the other three

694   provinces, Jiangsu and Anhui had relatively high flood risks, reaching 0.525 and 0.516, respectively, in

695   2020, whereas Zhejiang had a relatively low flood risk, which remained stable between 1990 and 2010,

696   with no distinct changes.

697
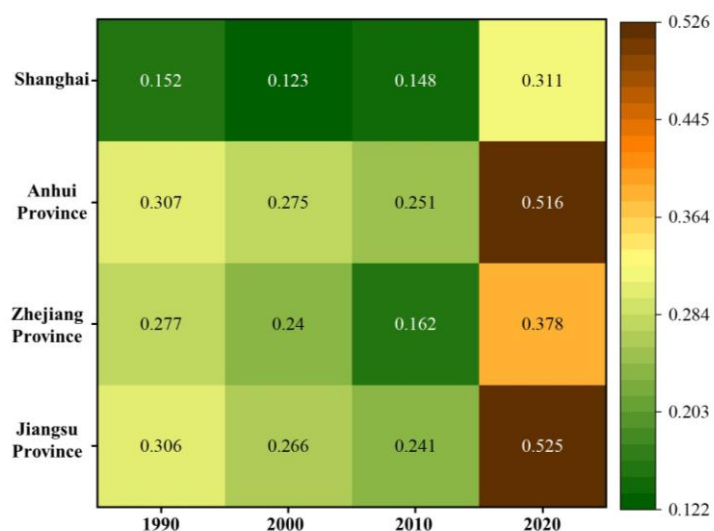
Figure 12: Distribution of Average Flood Risk in Each Province of the Yangtze River Delta Urban

Agglomeration from 1990 to 2020

700

4 Conclusion

Flood risk assessment at the scale of urban agglomeration is a hot research topic in the field of disaster

prevention and mitigation. In this study, the flood risk assessment indexes for YRDUA were determined

in different dimensions of danger, exposure, vulnerability and resilience, and a flood risk assessment

model based on AutoML and AHP was constructed to study the changes of spatial and temporal

characteristics of flood risk in the region in the last 30 years from 1990 to 2020, aiming to provide

scientific basis for the prevention and resilience of the YRDUA. The main conclusions of this study are

as follows:

(1) In the flood risk calculation, the CatBoost model has the highest Precision, F1-score, and Kappa, and

its Precision can reach 0.9030. Further analysis of the ROC curve and the corresponding AUC value of

the model shows that its AUC value is 0.91, which indicates that the CatBoost model has the best

performance and prediction reliability. Therefore, the CatBoost model was selected to calculate the flood

risk in the YRDUA.

714   (2) Using the flood risk assessment model based on AutoML and AHP to obtain the flood risk of the

715   YRDUA, superimposed on the flooded point data for comparative analysis, we found that the distribution

716   of flooded points in the study area is basically consistent with the distribution of high and medium-to-

717   high risk areas of flooding, and the proportion of the distribution of the quantification of its distribution

718   is 87.45%, which indicates that the model in this study has a good performance and credibility regarding

719   the assessment of flood risk.

720   (3) The spatial distribution of flood risk in the YRDUA during the 30-year study period shows obvious

721   heterogeneity, with the southwestern part of the region and Shanghai City having a low flood risk,

722   whereas the north-central part of the region faces a relatively high probability of flood risk. Between

723   1990 and 2010, there was a substantial decrease in the high and medium-to-high risk flood zones; yet by

724   2020, there was an increase in the high-risk flood zones. There is a tendency for the medium-to-high risk

725   area in the center of the region to shift to a high-risk area, whereas high-risk areas also occur in the cities

726   of Chizhou and Anqing in Anhui Province.

727   (4) All administrative units of the YRDUA exhibited the highest flood risk in 2020, with an overall trend

728   of increasing risk. At the provincial level, Jiangsu and Anhui Provinces possess relatively high flood

729   risks, whereas Zhejiang Province has a relatively low flood risk.

730   (5) The findings of this study provide valuable insights for flood risk management and policy-making.

731   The flood risk maps generated in this study can serve as a scientific basis for urban planning,

732   infrastructure development, emergency response, and disaster prevention strategies. By integrating these

733   risk assessments into decision-making processes, government agencies and urban planners can optimize

734   flood prevention measures and enhance regional resilience. Furthermore, the AutoML framework used

735   in this study can be applied to other regions for flood risk assessment and can be integrated with future

736   climate change scenarios to enable long-term forecasting and proactive disaster mitigation strategies.

737   **Data availability.**

738   Data will be made available on request.

739   Administrative boundaries and river network density were obtained from the Resource and

740   Environmental Science and Data Center, Chinese Academy of Sciences

741   (https://www.resdc.cn/DataList.aspx). Digital elevation data were derived from the SRTM1 dataset

provided by USGS (https://earthexplorer.usgs.gov/). Land use data were sourced from the China Land Cover Dataset (CLCD) developed by Wuhan University (https://zenodo.org/records/8176941). Hourly precipitation data from 120 meteorological stations were obtained from the National Meteorological Information Center, China Meteorological Administration (https://data.cma.cn/). Historical flood inundation data were obtained from the MODIS-based Global Flood Database and validated using the EM-DAT disaster database (https://developers.google.com/earthengine/datasets/catalog/GLOBAL_FLOOD_DB_MODIS_EVENTS_V1).

Competing interests.

The authors declare that they have no competing financial interests or personal relationships that may have influenced the work reported in this study.

Author contributions.

~~Yu Gao~~YG: Writing - original draft preparation, Validation, Software, Methodology, Conceptualization ~~Haipeng Lu~~HL: Writing-review & editing, Visualization, Supervision, Formal analysis. ~~Yaru Zhang~~YZ: Methodology, Formal analysis. ~~Hengxu Jin~~HJ: Writing - review & editing, Methodology. ~~Shuai Wu~~SW: Software, Formal analysis. ~~Yixuan Gao~~YG: Visualization, Software. ~~Shuliang Zhang~~SZ: Writing-review & editing, Resources, Project administration, Funding acquisition, Conceptualization .

Acknowledgements

This study was supported by the National Natural Science Foundation of China (Grant Nos. 42271483 and 42071364) and Jiangsu Provincial Natural Resources Science and Technology Project (JSZRKJ202405). We would like to thank Editage (www.editage.cn) for English language editing.

764 **References**

765 Abu-Salih, B., Wongthongtham, P., Coutinho, K., Qaddoura, R., Alshaweesh, O., and Wedyan, M.: The

766 development of a road network flood risk detection model using optimised ensemble learning, Eng. Appl.

767 Artif. Intell., 122, 106081, https://doi.org/10.1016/j.engappai.2023.106081, 2023.

768 Adnan, R. M., Yuan, X., Kisi, O., and Anam, R.: Improving Accuracy of River Flow Forecasting Using

769 LSSVR with Gravitational Search Algorithm, Advances in Meteorology, 2017, 1–23,

770 https://doi.org/10.1155/2017/2391621, 2017.

771 Anon: Identification of sensitivity indicators of urban rainstorm flood disasters: A case study in China,

772 J. Hydrology., 599, 126393, https://doi.org/10.1016/j.jhydrol.2021.126393, 2021.

773 Aven, T.: Risk assessment and risk management: Review of recent advances on their foundation,

774 European Journal of Operational Research, 253, 1–13, https://doi.org/10.1016/j.ejor.2015.12.023, 2016.

775 Bostan, P. A., Heuvelink, G. B. M., and Akyurek, S. Z.: Comparison of regression and kriging techniques

776 for mapping the average annual precipitation of Turkey, Int. J. Appl. Earth Obs. Geoinf., 19, 115–126,

777 https://doi.org/10.1016/j.jag.2012.04.010, 2012.

778 Consuegra-Ayala, J. P., Gutiérrez, Y., Almeida-Cruz, Y., and Palomar, M.: Intelligent ensembling of

779 auto-ML system outputs for solving classification problems, Inform. Sci., 609, 766–780,

780 https://doi.org/10.1016/j.ins.2022.07.061, 2022.

781 Cressie, N.: The origins of kriging, Math Geol, 22, 239–252, https://doi.org/10.1007/BF00889887, 1990.

782 Criado, M., Martínez-Graña, A., San Román, J. S., and Santos-Francés, F.: Flood risk evaluation in urban

783 spaces: The study case of Tormes River (Salamanca, Spain), International journal of environmental

784 research and public health, 16, 5, 2019.

785 Ding, T., Chen, J., Fang, Z., and Chen, J.: Assessment of coordinative relationship between

786 comprehensive ecosystem service and urbanization: A case study of Yangtze River Delta urban

787 Agglomerations, China, Ecol. Indic., 133, 108454, https://doi.org/10.1016/j.ecolind.2021.108454, 2021.

788 Donegan, H. A., Dodd, F. J., and McMaster, T. B. M.: A New Approach to Ahp Decision-Making,

789 Journal of the Royal Statistical Society: Series D (The Statistician), 41, 295–302,

790 https://doi.org/10.2307/2348551, 1992.

791 Echendu, A. J.: The impact of flooding on Nigeria's sustainable development goals (SDGs), Ecosyst.

792 Health Sustainability, 6, 1791735, https://doi.org/10.1080/20964129.2020.1791735, 2020.

793   Fernández, D. S. and Lutz, M. A.: Urban flood hazard zoning in Tucumán Province, Argentina, using

794   GIS and multicriteria decision analysis, Eng. Geol., 111, 90–98, 2010.

795   Gain, A. K., Mojtahed, V., Biscaro, C., Balbi, S., and Giupponi, C.: An integrated approach of flood risk

796   assessment in the eastern part of Dhaka City, Nat. Hazards, 79, 1499–1530,

797   https://doi.org/10.1007/s11069-015-1911-7, 2015.

798   Gu, C., Hu, L., Zhang, X., Wang, X., and Guo, J.: Climate change and urbanization in the Yangtze River

799   Delta, Habitat Int., 35, 544–552, https://doi.org/10.1016/j.habitatint.2011.03.002, 2011.

800   Guan, X., Yu, F., Xu, H., Li, C., and Guan, Y.: Flood risk assessment of urban metro system using

801   random forest algorithm and triangular fuzzy number based analytical hierarchy process approach,

802   Sustainable Cities and Society, 109, 105546, https://doi.org/10.1016/j.scs.2024.105546, 2024.

803   Gudiyangada Nachappa, T., Tavakkoli Piralilou, S., Gholamnia, K., Ghorbanzadeh, O., Rahmati, O., and

804   Blaschke, T.: Flood susceptibility mapping with machine learning, multi-criteria decision analysis and

805   ensemble using Dempster Shafer Theory, Journal of Hydrology, 590, 125275,

806   https://doi.org/10.1016/j.jhydrol.2020.125275, 2020.

807   Guo, Y., Quan, L., Song, L., and Liang, H.: Construction of rapid early warning and comprehensive

808   analysis models for urban waterlogging based on AutoML and comparison of the other three machine

809   learning algorithms, J. Hydrol., 605, 127367, 2022a.

810   Guo, Y., Quan, L., Song, L., and Liang, H.: Construction of rapid early warning and comprehensive

811   analysis models for urban waterlogging based on AutoML and comparison of the other three machine

812   learning algorithms, J. Hydrol., 605, 127367, https://doi.org/10.1016/j.jhydrol.2021.127367, 2022b.

813   Guo, Y., Quan, L., Song, L., and Liang, H.: Construction of rapid early warning and comprehensive

814   analysis models for urban waterlogging based on AutoML and comparison of the other three machine

815   learning algorithms, Journal of Hydrology, 605, 127367, https://doi.org/10.1016/j.jhydrol.2021.127367,

816   2022c.

817   He, X., Zhao, K., and Chu, X.: AutoML: A survey of the state-of-the-art, Knowledge-Based Systems,

818   212, 106622, https://doi.org/10.1016/j.knosys.2020.106622, 2021a.

819   He, X., Zhao, K., and Chu, X.: AutoML: A survey of the state-of-the-art, Knowledge-Based Systems,

820   212, 106622, https://doi.org/10.1016/j.knosys.2020.106622, 2021b.

821 Hites, R., De Smet, Y., Risse, N., Salazar-Neumann, M., and Vincke, P.: About the applicability of

822 MCDA to some robustness problems, European Journal of Operational Research, 174, 322–332,

823 https://doi.org/10.1016/j.ejor.2005.01.031, 2006.

824 Hsiao, S.-C., Chiang, W.-S., Jang, J.-H., Wu, H.-L., Lu, W.-S., Chen, W.-B., and Wu, Y.-T.: Flood risk

825 influenced by the compound effect of storm surge and rainfall under climate change for low-lying coastal

826 areas, Science of the total environment, 764, 144439, 2021.

827 Hutter, F., Kotthoff, L., and Vanschoren, J. (Eds.): Automated Machine Learning: Methods, Systems,

828 Challenges, Springer Nature, https://doi.org/10.1007/978-3-030-05318-5, 2019.

829 Jordan, M. and Mitchell, T.: Machine learning: Trends, perspectives, and prospects, Science, 349, 255–

830 260, https://doi.org/10.1126/science.aaa8415, 2015.

831 Kanani-Sadat, Y., Arabsheibani, R., Karimipour, F., and Nasseri, M.: A new approach to flood

832 susceptibility assessment in data-scarce and ungauged regions based on GIS-based hybrid multi criteria

833 decision-making method, J. Hydrol., 572, 17–31, https://doi.org/10.1016/j.jhydrol.2019.02.034, 2019.

834 Kazienko, P., Lughofer, E., and Trawinski, B.: Editorial on the special issue "Hybrid and ensemble

835 techniques in soft computing: recent advances and emerging trends," Soft Computing., 19, 3353–3355,

836 https://doi.org/10.1007/s00500-015-1916-x, 2015.

837 Khadka, D., Babel, M. S., and Kamalamma, A. G.: Assessing the Impact of Climate and Land-Use

838 Changes on the Hydrologic Cycle Using the SWAT Model in the Mun River Basin in Northeast Thailand,

839 Water, 15, 3672, https://doi.org/10.3390/w15203672, 2023.

840 Khosravi, K., Shahabi, H., Pham, B. T., Adamowski, J., Shirzadi, A., Pradhan, B., Dou, J., Ly, H.-B.,

841 Gróf, G., Ho, H. L., Hong, H., Chapi, K., and Prakash, I.: A comparative assessment of flood

842 susceptibility modeling using Multi-Criteria Decision-Making Analysis and Machine Learning Methods,

843 J. Hydrol., 573, 311–323, https://doi.org/10.1016/j.jhydrol.2019.03.073, 2019.

844 Lang, M., Barriendos, M., Llasat, M. C., Francés, F., Ouarda, T., Thorndycraft, V., Enzel, Y., Bardossy,

845 A., Coeur, D., and Bobée, B.: Use of Systematic, Palaeoflood and Historical Data for the Improvement

846 of Flood Risk Estimation. Review of Scientific Methods, Nat. Hazards, 31, 623–643,

847 https://doi.org/10.1023/B:NHAZ.0000024895.48463.eb, 2004.

848 Li, J., Cheng, K., Wang, S., Morstatter, F., Trevino, R. P., Tang, J., and Liu, H.: Feature Selection: A

849 Data Perspective, ACM Comput. Surv., 50, 94:1-94:45, https://doi.org/10.1145/3136625, 2017.

Lin, L., Wu, Z., and Liang, Q.: Urban flood susceptibility analysis using a GIS-based multi-criteria analysis framework, Nat Hazards, 97, 455–475, https://doi.org/10.1007/s11069-019-03615-2, 2019.

Liu Jiafu and Zhang Bai: Progress of Rainstorm Flood Risk Assessment, Geographical Science, 35, 346–351, https://doi.org/10.13249/j.cnki.sgs.2015.03.013, 2015.

Lu, H., Lu, X., Jiao, L., and Zhang, Y.: Evaluating urban agglomeration resilience to disaster in the Yangtze Delta city group in China, Sustainable Cities and Society, 76, 103464, 2022.

Lundberg, S. M. and Lee, S.-I.: A Unified Approach to Interpreting Model Predictions, in: Advances in Neural Information Processing Systems, 2017.

Ma, C., Chen, Z., Zhao, K., Xu, H., and Qi, W.: Improved urban flood risk assessment based on spontaneous-triggered risk assessment conceptual model considering road environment, Journal of Hydrology, 608, 127693, https://doi.org/10.1016/j.jhydrol.2022.127693, 2022.

Mahmoud, S. H. and Gan, T. Y.: Urbanization and climate change implications in flood risk management: Developing an efficient decision support system for flood susceptibility mapping, Science of The Total Environment, 636, 152–167, https://doi.org/10.1016/j.scitotenv.2018.04.282, 2018.

Mia, Md. U., Rahman, M., Elbeltagi, A., Abdullah-Al-Mahbub, Md., Sharma, G., Islam, H. M. T., Pal, S. C., Costache, R., Islam, A. R. Md. T., Islam, M. M., Chen, N., Alam, E., and Washakh, R. M. A.: Sustainable flood risk assessment using deep learning-based algorithms with a blockchain technology, Geocarto International, 38, 1–29, https://doi.org/10.1080/10106049.2022.2112982, 2023.

Milanesi, L., Pilotti, M., and Ranzi, R.: A conceptual model of people's vulnerability to floods, Water Resources Res., 51, 182–197, https://doi.org/10.1002/2014WR016172, 2015.

Mirzaei, S., Vafakhah, M., Pradhan, B., and Alavi, S. J.: Flood susceptibility assessment using extreme gradient boosting (EGB), Iran, Earth Sci. Inf., 14, 51–67, https://doi.org/10.1007/s12145-020-00530-0, 2021.

Mishra, K. and Sinha, R.: Flood risk assessment in the Kosi megafan using multi-criteria decision analysis: A hydro-geomorphic approach, Geomorphology, 350, 106861, https://doi.org/10.1016/j.geomorph.2019.106861, 2020.

Morales-Torres, A., Escuder-Bueno, I., Andrés-Doménech, I., and Perales-Momparler, S.: Decision Support Tool for energy-efficient, sustainable and integrated urban stormwater management, Environmental Modelling & Software, 84, 518–528, https://doi.org/10.1016/j.envsoft.2016.07.019, 2016.

880 Munim, Z. H., Sørli, M. A., Kim, H., and Alon, I.: Predicting maritime accident risk using Automated

881 Machine Learning, Reliab. Eng. Syst. Saf., 248, 110148, https://doi.org/10.1016/j.ress.2024.110148,

882 2024.

883 Nagarajah, T. and Poravi, G.: A Review on Automated Machine Learning (AutoML) Systems, in: 2019

884 IEEE 5th International Conference for Convergence in Technology (I2CT), 2019 IEEE 5th International

885 Conference   for   Convergence   in   Technology   (I2CT),   1–6,

886 https://doi.org/10.1109/I2CT45611.2019.9033810, 2019.

887 Nayak, P. C., Sudheer, K. P., Rangan, D. M., and Ramasastri, K. S.: A neuro-fuzzy computing technique

888 for modeling hydrological time series, J. Hydrol., 291, 52–66, 2004.

889 Özdemir, H., Baduna Koçyiğit, M., and Akay, D.: Flood susceptibility mapping with ensemble machine

890 learning: a case of Eastern Mediterranean basin, Türkiye, Stoch. Env. Res. Risk A., 37, 4273–4290,

891 https://doi.org/10.1007/s00477-023-02507-z, 2023.

892 Pham, B. T., Luu, C., Dao, D. V., Phong, T. V., Nguyen, H. D., Le, H. V., von Meding, J., and Prakash,

893 I.: Flood risk assessment using deep learning integrated with multi-criteria decision analysis, Knowledge-

894 Based Systems, 219, 106899, https://doi.org/10.1016/j.knosys.2021.106899, 2021.

895 Raschka, S.: Model Evaluation, Model Selection, and Algorithm Selection in Machine Learning,

896 https://doi.org/10.48550/arXiv.1811.12808, 10 November 2020.

897 Rashidi Shikhteymour, S., Borji, M., Bagheri-Gavkosh, M., Azimi, E., and Collins, T. W.: A novel

898 approach for assessing flood risk with machine learning and multi-criteria decision-making methods,

899 Appl. Geogr., 158, 103035, https://doi.org/10.1016/j.apgeog.2023.103035, 2023.

900 Saaty, T. L.: The Analytic Hierarchy Process: Decision Making in Complex Environments, in:

901 Quantitative Assessment in Arms Control: Mathematical Modeling and Simulation in the Analysis of

902 Arms Control Problems, edited by: Avenhaus, R. and Huber, R. K., Springer US, Boston, MA, 285–308,

903 https://doi.org/10.1007/978-1-4613-2805-6_12, 1984.

904 Sarro, F., Moussa, R., Petrozziello, A., and Harman, M.: Learning From Mistakes: Machine Learning

905 Enhanced   Human   Expert   Effort   Estimates,   IEEE   Trans.   Softw.   Eng.,   48,   1868–1882,

906 https://doi.org/10.1109/TSE.2020.3040793, 2022.

907 Scott, D., Hall, C. M., Rushton, B., and Gössling, S.: A review of the IPCC Sixth Assessment and

908 implications for tourism development and sectoral climate action, J. Sustain. Tour., 0, 1–18,

909 https://doi.org/10.1080/09669582.2023.2195597, 2023.

910   Seemuangngam, A. and Lin, H.-L.: The impact of urbanization on urban flood risk of Nakhon

911   Ratchasima, Thailand, Appl. Geogr., 162, 103152, https://doi.org/10.1016/j.apgeog.2023.103152, 2024.

912   Shafizadeh-Moghadam, H., Valavi, R., Shahabi, H., Chapi, K., and Shirzadi, A.: Novel forecasting

913   approaches using combination of machine learning and statistical models for flood susceptibility

914   mapping, Journal of environmental management, 217, 1–11, 2018.

915   Shuster, W. D., Bonta, J., Thurston, H., Warnemuende, E., and Smith, D. R.: Impacts of impervious

916   surface on watershed hydrology: A review, Urban Water Journal,

917   https://doi.org/10.1080/15730620500386529, 2005.

918   Sinha, R., Bapalu, G. V., Singh, L. K., and Rath, B.: Flood risk analysis in the Kosi river basin, north

919   Bihar using multi-parametric approach of Analytical Hierarchy Process (AHP), J. Indian Soc. Remote

920   Sens., 36, 335–349, https://doi.org/10.1007/s12524-008-0034-y, 2008.

921   Sun, B., Fang, C., Liao, X., Guo, X., and Liu, Z.: The relationship between urbanization and air pollution

922   affected by intercity factor mobility: A case of the Yangtze River Delta region, Environ. Impact Assess.

923   Rev., 100, 107092, https://doi.org/10.1016/j.eiar.2023.107092, 2023.

924   Tang, Z., Wang, P., Li, Y., Sheng, Y., Wang, B., Popovych, N., and Hu, T.: Contributions of climate

925   change and urbanization to urban flood hazard changes in China's 293 major cities since 1980, J.

926   Environ. Manage., 353, 120113, https://doi.org/10.1016/j.jenvman.2024.120113, 2024.

927   Vincent, A. M., K.s.s., P., and Jidesh, P.: Flood susceptibility mapping using AutoML and a deep learning

928   framework with evolutionary algorithms for hyperparameter optimization, Applied Soft Computing.,

929   148, 110846, https://doi.org/10.1016/j.asoc.2023.110846, 2023.

930   Wagenaar, D., Curran, A., Balbi, M., Bhardwaj, A., Soden, R., Hartato, E., Mestav Sarica, G., Ruangpan,

931   L., Molinario, G., and Lallemant, D.: Invited perspectives: How machine learning will change flood risk

932   and impact assessment, Nat. Hazard. Earth Sys., 20, 1149–1161, https://doi.org/10.5194/nhess-20-1149-

933   2020, 2020.

934   Wan, H., Zhong, Z., Yang, X., and Li, X.: Impact of city belt in Yangtze River Delta in China on a

935   precipitation process in summer: A case study, Atmos. Res., 125–126, 63–75,

936   https://doi.org/10.1016/j.atmosres.2013.02.004, 2013.

937   Wang, M., Fu, X., Zhang, D., Chen, F., Liu, M., Zhou, S., Su, J., and Tan, S. K.: Assessing urban flooding

938   risk in response to climate change and urbanization based on shared socio-economic pathways, Science

939   of The Total Environment, 880, 163470, https://doi.org/10.1016/j.scitotenv.2023.163470, 2023a.

940 Wang, P., Deng, X., Zhou, H., and Qi, W.: Responses of urban ecosystem health to precipitation extreme:

941 A case study in Beijing and Tianjin, Journal of Cleaner Production, 177, 124–133,

942 https://doi.org/10.1016/j.jclepro.2017.12.125, 2018a.

943 Wang, P., Li, Y., Yu, P., and Zhang, Y.: The analysis of urban flood risk propagation based on the

944 modified susceptible infected recovered model, J. Hydrology., 603, 127121,

945 https://doi.org/10.1016/j.jhydrol.2021.127121, 2021.

946 Wang, T., Wang, H., Wang, Z., and Huang, J.: Dynamic risk assessment of urban flood disasters based

947 on functional area division—A case study in Shenzhen, China, J. Environ. Manage., 345, 118787,

948 https://doi.org/10.1016/j.jenvman.2023.118787, 2023b.

949 Wang, Y., Liu, G., Guo, E., and Yun, X.: Quantitative Agricultural Flood Risk Assessment Using

950 Vulnerability Surface and Copula Functions, Water, 10, 1229, https://doi.org/10.3390/w10091229,

951 2018b.

952 Wang, Y., Li, C., Hu, Y., Lv, J., Liu, M., Xiong, Z., and Wang, Y.: Evaluation of urban flooding and

953 potential exposure risk in central and southern Liaoning urban agglomeration, China, Ecological

954 Indicators, 154, 110845, https://doi.org/10.1016/j.ecolind.2023.110845, 2023c.

955 Webb, G. I. and Zheng, Z.: Multistrategy ensemble learning: reducing error by combining ensemble

956 learning techniques, IEEE Transactions on Knowledge and Data Engineering, 16, 980–991,

957 https://doi.org/10.1109/TKDE.2004.29, 2004.

958 Webster, R. and Oliver, M. A.: Geostatistics for Environmental Scientists, John Wiley & Sons, 333 pp.,

959 2007.

960 Wolpert, D. H. and Macready, W. G.: No free lunch theorems for optimization, IEEE Transactions on

961 Evolutionary Computation, 1, 67–82, https://doi.org/10.1109/4235.585893, 1997.

962 Xu, H., Hou, X., Pan, S., Bray, M., and Wang, C.: Socioeconomic impacts from coastal flooding in the

963 21st century China's coastal zone: A coupling analysis between coastal flood risk and socioeconomic

964 development, Sci. Total Environ., 917, 170187, 2024.

965 Yan, M., Yang, J., Ni, X., Liu, K., Wang, Y., and Xu, F.: Urban waterlogging susceptibility assessment

966 based on hybrid ensemble machine learning models: A case study in the metropolitan area in Beijing,

967 China, J. Hydrol., 630, 130695, 2024.

968   Yang, J., Zeng, X., Zhong, S., and Wu, S.: Effective Neural Network Ensemble Approach for Improving

969   Generalization Performance, IEEE Transactions on Neural Networks and Learning Systems, 24, 878–

970   887, https://doi.org/10.1109/TNNLS.2013.2246578, 2013.

971   Yang, W., Xu, K., Lian, J., Ma, C., and Bin, L.: Integrated flood vulnerability assessment approach based

972   on TOPSIS and Shannon entropy methods, Ecol. Indic., 89, 269–280,

973   https://doi.org/10.1016/j.ecolind.2018.02.015, 2018.

974   Yang, X., Li, H., Zhang, J., Niu, S., and Miao, M.: Urban economic resilience within the Yangtze River

975   Delta urban agglomeration: Exploring spatially correlated network and spatial heterogeneity, Sustainable

976   Cities and Society, 103, 105270, https://doi.org/10.1016/j.scs.2024.105270, 2024.

977   Yuan, X., Chen, C., Lei, X., Yuan, Y., and Muhammad Adnan, R.: Monthly runoff forecasting based on

978   LSTM–ALO model, Stoch. Env. Res. Risk A., 32, 2199–2212, https://doi.org/10.1007/s00477-018-

979   1560-y, 2018.

980   Zhang, H., Wu, C., Chen, W., and Huang, G.: Assessing the Impact of Climate Change on the

981   Waterlogging Risk in Coastal Cities: A Case Study of Guangzhou, South China,

982   https://doi.org/10.1175/JHM-D-16-0157.1, 2017.

983